Multiscale simulations of primary atomization

G. Tomar[a,b], D. Fuster[a,b], S. Zaleski[a,b*] and S. Popinet[c]
[a]UPMC Univ Paris 06, UMR 7190, Institut Jean Le Rond d'Alembert, F-75005, Paris, France.
[b]CNRS, UMR 7190, Institut Jean Le Rond d'Alembert, F-75005 Paris, France.
[c]NIWA, P.O. Box 14-901, Kilbirnie, Wellington, New Zealand.

Abstract

Atomization of a liquid jet by a high speed air stream flowing over it is a phenomenon of paramount importance to industrial applications. The probability density function (PDF) of the droplet size distribution in atomization has been a subject of keen interest as it is a measure of atomization efficiency. Further, the trajectory of the droplets as they detach and disperse away from the jet is also important. Numerical simulations resolving the smallest droplets are exceedingly expensive computationally. We present here, a Lagrangian tracking algorithm coupled with a VOF algorithm to transform smallest droplets into particles to be modeled as Lagrangian particles. The influence of the droplets on the flow is accounted for by using a momentum source term in the Navier-Stokes equation. We show that the droplets maintain a near linear trajectory as they pass through the gas jet. A PDF of the droplet distribution in different regions suggests different mechanisms generating droplets at different scales and show the evolution of the PDF in space.

Introduction

A large set of physical systems of industrial and scientific relevance involve interactions between phenomena occurring at various scales. Disparate scales are seen in situations like micro and nano-fluidics, particle-laden flows, combustion chambers, spray drying and atmospheric flows [1, 2]. Numerical simulations of a physical process involving temporal and spatial scales separated by orders of magnitude require huge computational resources and time. In atomization, a liquid jet breaks up into small droplets because of interplay of several mechanisms active in the atomization process. The droplets broken-off from the liquid jet are orders of magnitude smaller than its diameter. With the advent of various sharp-interface-tracking algorithms [3–9], numerical simulations of the atomization process have become possible[10–12]. Three dimensional temporal simulations of the breakup of a liquid jet by a coaxial high-speed gas have been reported in Refs.[10, 13] using the Volume-of-Fluid (VOF) method and by Tauber et al. [11] using the Front-Tracking method. Both studies showed the formation of thin ligaments which subsequently break into droplets. Small droplets formed during the atomization process require high grid resolution thus increasing the computational cost by several folds. The computational cost can be reduced by artificially removing the smallest droplets from regions of the computational domain far from the liquid jet. An unaccounted removal of the droplets formed might affect the measurements of probability density function (PDF) of droplets and further may also lead to the loss of physics. Thus, a multiscale model is required to incorporate the essential effects of the droplet without investing enormous computational effort in completely resolving all the involved scales using a Navier Stokes solver. Recently, Kim et al. [12] performed multiscale simulations of a primary breakup of a liquid jet by a coaxial flow of gas. A variant of the Level-Set method was employed to solve the two-phase flow coupled with a Lagrangian spray model to track the droplets broken-off from the liquid jet. However, the splashing of the droplets on the primary jet was not modeled.

We present here, multiscale simulations of a primary jet breakup using an Eulerian-Lagrangian approach with two-way coupling, that is, both-way interaction between fluid and particles. The method has been implemented in Gerris [14], a two-phase VOF solver with balanced force surface tension model and quad/octree adaptive mesh refinement. The momentum source term in the Navier-Stokes equation because of the particles is smoothed using a Gaussian distribution function. The algorithm has been validated against various test cases. Finally, we present simulations of a breakup of a liquid jet converting droplets into particles upon formation and back into VOF resolved droplets based on their proximity to the VOF interface. We present a PDF of the droplet sizes during the atomization process.

*Email: stephane.zaleski@upmc.fr, Tel: +33 1 44272558, Fax: +33 1 44275259.

Formulation

The Navier-Stokes equations for a two-phase incompressible flow modified to implicitly incorporate the boundary conditions at the interface can be written as,

$$\rho[\partial_t \boldsymbol{u} + (\boldsymbol{u}\bullet\nabla)\boldsymbol{u}] = -\nabla p + \nabla\bullet\left(2\mu\boldsymbol{D}\right) + \sigma\kappa\delta_s\boldsymbol{n} + \boldsymbol{\Phi}_p, \quad (1)$$

where $\boldsymbol{u} = (u,v,w)$ is the fluid velocity, $\rho(\boldsymbol{x},t)$ is the fluid density, $\mu(\boldsymbol{x},t)$ is the dynamic viscosity and $\boldsymbol{D}$, the deformation tensor, is defined as $\boldsymbol{D} = \left(\left(\nabla\boldsymbol{u}\right) + \left(\nabla\boldsymbol{u}\right)^T\right)/2$. The surface tension force is non-zero only at the interface as signified by the Dirac delta function, δ_s, with σ, $\boldsymbol{n}$ and κ representing the surface tension coefficient, the unit normal and the curvature at the interface, respectively. The momentum source term $\boldsymbol{\Phi}_p$ represents the effect of the dispersed phase simulated using a Lagrangian approach.

The advection equation for density and the incompressibility condition are given by,

$$\partial_t \rho + \nabla\bullet(\rho\boldsymbol{u}) = 0, \quad (2)$$

$$\nabla\bullet\boldsymbol{u} = 0. \quad (3)$$

The density and the viscosity field are obtained as,

$$\rho \equiv c\rho_1 + (1-c)\rho_2 \quad \text{and} \quad (4)$$

$$\mu \equiv c\mu_1 + (1-c)\mu_2, \quad (5)$$

respectively, where $c(\boldsymbol{x},t)$ is the volume fraction. Here, ρ_1, ρ_2 and μ_1, μ_2 are the densities and viscosities of the first and second fluids, respectively. The volume fraction takes values between zero and one. The advection equation for the density can be written in terms of the volume fraction as,

$$\partial_t c + \nabla\bullet(c\boldsymbol{u}) = 0. \quad (6)$$

A two-way coupled Eulerian-Lagrangian approach for the dispersed phase comprises of computing the external and fluid forces on the particle and incorporating the effect of the particles as a source term in the Navier-Stokes equation ($\boldsymbol{\Phi}_p$). The governing equations of the motion of the particles are given by,

$$\frac{d\boldsymbol{x}_i}{dt} = \boldsymbol{v}_i, \quad (7)$$

$$m_i \frac{dv_i}{dt} = F_D + F_I + F_A + F_L + F_{ext}. \quad (8)$$

where, m_i, $\boldsymbol{x}_i$ and $\boldsymbol{v}_i$ are the mass, position and the velocity of the i−th particle respectively. The density and volume of the particle are denoted by ρ_p^i and V^i, respectively. The different forces $F_D, F_I, F_A, F_L, F_{ext}$, acting on the particle are the drag, inertial, added mass force, lift and external forces, respectively (see Refs [15,16] for details).

The momentum source term $\boldsymbol{\Phi}_p$ in the Eq.1 is given by,

$$\boldsymbol{\Phi}_p = \lim_{V_f\to 0}\sum_{i=1}^{N_p}\frac{V^i}{V_f}\left[\rho_p^i\left(\boldsymbol{g} - \frac{d\boldsymbol{v}^i}{dt}\right) + \rho\left(\frac{D\boldsymbol{u}}{Dt} - \boldsymbol{g}\right)\right], \quad (9)$$

where V_f is the control volume containing N_p particles [15].

The methodology adopted for solving the two-phase, sharp-interface, incompressible flow equations is presented in detail in Refs.[14, 17, 18]. A second-order accurate staggered in time discretisation has been employed for the volume-fraction/density and pressure fields. The details of the algorithm and its validation are presented elsewhere [18]. The Lagrangian particle tracking is performed using the updated velocity field. The fluid forces which are a function of the relative velocity between the particle and the fluid are computed. The fluid velocity is obtained at the particle position using a bilinear interpolation. Acceleration (Eq. 8) so obtained is integrated to compute the velocity of the particle and subsequently the updated particle position (Eq. 7). Equations 7 and 8 are discretized in time using the first order explicit forward Euler scheme.

The two-way coupling force is a momentum source term in the Navier-Stokes equation (Eq. 1). To achieve numerical convergence it is smoothed using a Gaussian distribution with standard deviation σ_p. The standard deviation for

the distribution of the force is taken to be the maximum of the radius of the particle and the size of the computational cell containing its center. The particle size is in general smaller than the cell-size except in special situations where the grid is extremely refined due to high vorticity or some other criterion. The smoothed force is given by,

$$\tilde{\mathbf{\Phi}}_p = \mathbf{\Phi}_p e^{-|x-x_p|^2/\sigma_p^2} / \left(\sqrt{2\pi}\sigma_p\right)^D, \tag{10}$$

where $\tilde{\mathbf{\Phi}}_p$ is the smoothed force and D is the dimension of the problem (2 in 2D). The smoothed force is distributed only in a surrounding stencil of approximately $3\sigma_p$ to reduce the computational cost. On a quad/octree grid we achieve the above criterion efficiently by moving to a coarser level till one of the cell-faces is at least $3\sigma_p$ distance from the particle thence the closest neighbors in 2 (3 in 3-dimensional) directions are identified and the children of these are traversed up to the finest level where the source term $\tilde{\mathbf{\Phi}}_p$ is defined.

A small Volume-of-fluid resolved droplet, formed during the numerical simulations of the primary atomization, leads to expensive computational effort with little gain. In the present study, we propose to model small droplets as Lagrangian particles. The center of the particle is located at the centroid of the droplet and the average momentum is computed to define the velocity of the particle. The void fraction field is re-assigned to remove the droplet from the computational domain. Similarly, a point particle formed from a droplet can be transformed back into a VOF-resolved droplet based on its proximity to the VOF interface or a pre-specified region. The two-way coupling force is replaced by the velocity impulse introduced in the computational domain upon the transformation of the particle into a VOF-resolved droplet. Subsequently, the refined computational grid containing the droplet is assigned a uniform velocity field corresponding to the momentum of the particle. The above approximation can be improved by choosing an approximate analytical solution for the flow field inside the droplet. In addition, we perform 2D computations. The restriction to 2D flow is not realistic everywhere but constitutes only a heuristic exploration of what can be done. The drag, lift and other force laws used for studying the motion of the droplets are, however, three-dimensional.

Results and Discussion

For validation of the implementation of the Lagrangian particle-tracking algorithm, the motion of a particle computed using Gerris is compared with the results obtained from the Runge-Kutta integration using a prescribed shear-flow field. The fluid velocity field is given by,

$u = -C_s \cos(\pi x)\sin(\pi y),$

$v = C_s \sin(\pi x)\cos(\pi y),$

where, C_s is chosen to be 0.1.

The drag coefficient used is a function of the local particle Reynolds number $\mathrm{Re_p}$ [16],

$$C_D = \begin{cases} 16\dfrac{1+0.15\sqrt{\mathrm{Re}_p}}{\mathrm{Re}_p} & \text{if } \mathrm{Re}_p < 50, \\ 48\dfrac{\mathrm{Re}_p - 2.21}{\mathrm{Re}_p^{3/2}} & \text{otherwise.} \end{cases} \tag{11}$$

The lift and added-mass force coefficients (C_L and C_M) are chosen to be 0.5[16]. Figure 1 shows the particle trajectory for different grid resolutions. The cross in the figure marks the center of the anti-clockwise vortex. The solution obtained from a second order Runge-Kutta scheme is overlapping the computational results obtained for a grid resolution of $2^8 \times 2^8$. The test case shows that the Lagrangian particle tracking algorithm accurately captures the motion of the particles.

Forces on the fluid due to particles are modeled as a source of momentum in the Navier-Stokes equation. The size of the particle being considerably smaller compared to the computational grid size, the source of momentum is a point-force. As discussed previously, we diffuse the force in a small region. Here, we discuss a test case to evaluate the numerical aspects of diffusing a point force in a small region. A point-source of momentum in a fluid leads to a jet of fluid flowing away from the source [19,20]. The flow generated is axi-symmetric with the line of force as the axis-of-symmetry. A non-dimensional analysis yields a Reynolds-number like parameter, $F/(2\pi\rho\upsilon^2)$, governing

the flow. Due to the point source of momentum, a jet is formed by the entrainment of the slow-moving fluid pushed rapidly away from the origin. Here, υ is the dynamic viscosity. The edge of the so formed jet can be defined conveniently by the position where the streamlines are at the minimum distance from the axis. The azimuthal coordinate of the minimum point of the streamlines can be obtained from the relation below,

$$F/(2\pi\rho\upsilon^2) = \frac{32}{3}\frac{\cos\theta_0}{\sin^2\theta_0} + \frac{4}{\cos^2\theta_0}\log\left(\frac{1-\cos\theta_0}{1+\cos\theta_0}\right) + \frac{8}{\cos\theta_0}. \quad (12)$$

Figures 2(a) and (b) show the streamlines for $F/(2\pi\rho\upsilon^2) = 50$ and the comparison in the computed axial-velocity with the analytical solution for different grid resolutions. The quad tree grid is refined in a small radius (<0.05) with levels 8, 9 and 10. The force F is diffused in a small region with a standard deviation $2h_{min}$ where h_{min} corresponds to the minimum grid width ($1/2^8$ for grid level 8). The flow develops in time to show variation of $\sim r^{-m}$ in space where $m = -1.468, -1.144$ and -0.974 for levels 8, 9 and 10, respectively. The theoretical result is $\theta_0 = 24^0 37'$ and we obtain $\theta_0 = 30^0 12'$ with a force diffused using a standard deviation of 2^{-10} (quad-tree level 10).

We show here a simulation of atomization using the implementation of the Lagrangian particle tracking coupled with the Navier-Stokes solver (*Gerris*). A liquid jet atomizes into small droplets by a high-speed coaxial air-jet flowing over it. Thin liquid ligaments form at the liquid-gas interface due to the instability. Subsequently, the ligament breaks up into droplets. The prediction of the droplet size distribution in an atomization process is of immense importance in several industrial applications. For example, the distribution of fuel in combustion chambers is critical to fuel economy. We have performed an atomization simulation, on a parallel machine using eight nodes, with small droplets transformed into Lagrangian particles. In order to perform simulations in parallel, special care needs to be taken in prescribing consistent identification numbers to the particles. Thus, enabling us to study the trajectory of droplets. A planar simulation of a liquid jet destabilized by a high-speed co-flowing gas has been performed. A thin tapered separator plate (Figure 3(a)) separates the liquid and gas flow near the inlet. The taper angle used in the present simulation is 7^0, the thickness of the separator plate at the inlet is e=150μm and the radius of the trailing edge is 20 μm. The flow parameters of the liquid and gas used are given in Table 1. The nondimensional parameters governing the process, namely, liquid-gas momentum ratio $M = \rho_g U_g^2 / \rho_l U_l^2$, gas and liquid Reynolds numbers ($\mathrm{Re}_g = \rho_g U_g \delta_g / \mu_g$ and $\mathrm{Re}_l = \rho_l U_l \delta_l / \mu_l$) and Weber number $We_g = \rho_g U_g^2 \delta_g / \sigma$ are 16, 2060, 5000 and 10.2, respectively. The boundary layer in the gas, $\delta_g = 6.05\,\mathrm{Re}_g^{-1/2} H_g$, at the nozzle inlet is a function of the Re_g and is prescribed at the nozzle inlet using an experimental correlation [21]. Here, H_g is the thickness of the gas-jet. A similar correlation has been used at the liquid inlet to obtain δ_l. The quad-tree level refinement used for computations is 11 thus the smallest grid size is $\sim 5\mu m$ and the interface is maintained at the finest level in the computation. The size of the computational domain is chosen to be 6cmX3cm. The refinement criteria used in the simulations is described in Ref.[18].

The smallest droplets in the computational domain that occupy less than 25 smallest computational cells are transformed into particles. The local computational grid upon transformation is coarsened. Figure 3(b) shows a snapshot of an atomization simulation performed in parallel with eight nodes. The blue dots in the figure represent droplets which have been modeled as Lagrangian particles. Droplets once formed are entrained into the fast moving air-stream and are scattered in a wider region. The particles formed from droplets are resolved again by VOF when they approach a VOF-resolved interface. Figure 4 show the particle trajectories of the droplets formed near the inlet. The color of the lines represents the diameter of the particles. The particle lines maintain a near constant angle ($\sim 18^0$)with the mean jet flow. A few particles have a shorter life span before they collapse back into the liquid jet. Figures 5(a) and 5(b) show the probability density distributions of the droplets in two different regions of the computational domain (a) close to the nozzle inlet and (b) far from it (marked in Fig. 3(b)). Figure 5(a) shows a rather sharp peak for a diameter (10−20 μm) and another smoother peak of the distribution for a diameter (40−50 μm). In contrast, Fig. 5(b) shows a clear peak of the distribution at ~ 80 μm suggesting formation of larger droplets away from the nozzle. The above PDFs, thus, delineate the two mechanisms of formation of droplets, namely, by primary atomization of the jet and another by break-up of bigger fragments of liquid in the downstream.

Conclusions

Multiscale simulations of atomization of a liquid jet into droplets have been presented. A Lagrangian particle tracking algorithm with two-way coupling has been used to capture the effect of smallest droplets formed during atomization. The objective of the current study was to present an algorithm coupling VOF and Lagrangian particle tracking with applications to simulations of atomization. A high liquid-gas density and viscosity ratio (~100) atomization has been simulated using Gerris. A study of the trajectory of the droplets shows a rather linear motion of the droplet in the gas at a mean angle of ~18^0. Performing PDF of the droplet in two different regions of the computational domain shows two different mechanisms of droplet formation. Primary atomization near the liquid jet leads to the formation of small droplets whereas further downstream from the nozzle bigger droplets are formed.

References

1. K. Kusano, A. Kawano, H. Hasegawa, International Conference on Computational Science, 2007.
2. V. I. Kolobov, R. R. Arslanbekon, A. V. Vasenkov, *International Conference on Computational Science*, 2007.
3. J. Brackbill, D. B. Kothe, C. Zemach, *J. Comput. Phys.* 100:335–354 (1992).
4. S. O. Unverdi, G. Tryggvason, *J. Comput. Phys.* 100: 25–37(1992).
5. M. Sussman, P. Smereka, S. Osher, *J. Comput. Phys.* , 114: 146–159 (1994).
6. S. Zaleski, J. Li, R. Scardovelli, G. Zanetti, *Proceedings of the IMACSCOST Conference on Computational Fluid Dynamics*, Lausanne Sept. 13-15, 1995.
7. S. Popinet, S. Zaleski, *Int. J. Numer. Meth. Fluids* 30:775-793 (1999).
8. J. E. Pilliod Jr, E. G. Puckett, *J. Comput. Phys.*, 199: 465-502 (2004).
9. Y. Renardy, M. Renardy, *J. Comput. Phys.*, 183:400-421 (2002).
10. F. K. Keller, J. Li, A. Vallet, D. Vandromme, S. Zaleski, *Proc. Sixth Int. Conf. on Liquid Atomization and Spray Systems*, Rouen, 1994, pp. 56–62.
11. W. Tauber, G. Tryggvason, *Comput. Fluid Dynamics J.*, 9:594 (2000).
12. D. Kim, M. Herrmann, P. Moin, *American Physical Society, 59th Annual Meeting of the APS Division of Fluid Dynamics*, November 19-21, 2006, p. FB.010.
13. S. Zaleski, T. Boeck, *International Conference on Liquid and Spray Systems*, Sorrento, Italy, 2003.
14. S. Popinet, *J. Comput. Phys.* , 190:572–600 (2003).
15. E. Climent, J. Magnaudet, *Phys. Fluids*, 18:103304 (2006).
16. J. Magnaudet, I. Eames, *Ann. Rev. Fluid Mech.*, 32: 659–708 (2000).
17. S. Popinet, An accurate adaptive solver for surface-tension-driven interfacial flows, *J. Comp. Phys.*, In press (2009).
18. D. Fuster, A. Bague, T. Boeck, L. Moyne, A. Leboissetier, S. Popinet, P. Ray, R. Scardovelli, S. Zaleski, Simulation of primary atomization with an octree adaptative mesh refinement and vof method, *Int. J. Multiphase Flow*, 35(6): 550-565 (2009).
19. G. K. Batchelor, An introduction to fluid dynamics, Cambridge Univ. Press, 1970.
20. L. D. Landau, *C.R. (Doklady) Acad. Sci. URSS*, 43: 286–288 (1944).
21. F. Ben Rayana, Contribution à l'étude des instabilités interfaciales liquide-gaz en atomisation assistée et taille de gouttes, Ph.D. thesis, Institut National Polytechnique de Grenoble (2007).

Table 1**.** Properties of the liquid and the coaxially flowing gas jet.

U_g / U_l (m/s)	ρ_g / ρ_l (Kg/m^3)	μ_g / μ_l (Pa.s)	δ_g / e (μ m)
20 / 0.5	10 / 1000	1.7×10^{-5} / 10^{-3}	175/150

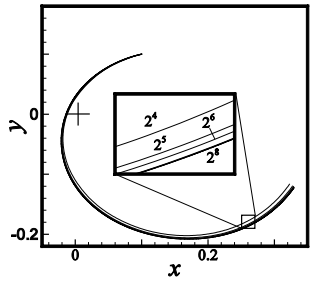

Figure 1. Particle tracking in a vortex flow

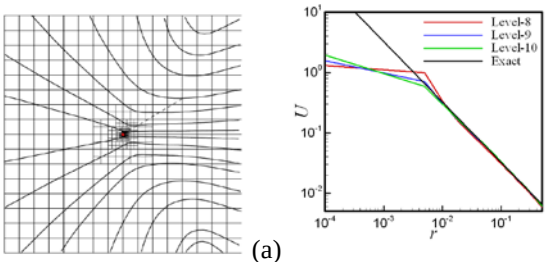

(a) (b)

Figure 2. (a) Streamlines for $F/(2\pi\rho\upsilon^2) = 50$ and the grid resolution around the point force is $1/2^{10}$ (b) Comparison of computed axial-velocity (at $\theta = 90^0$) for different resolutions with the analytical solution.

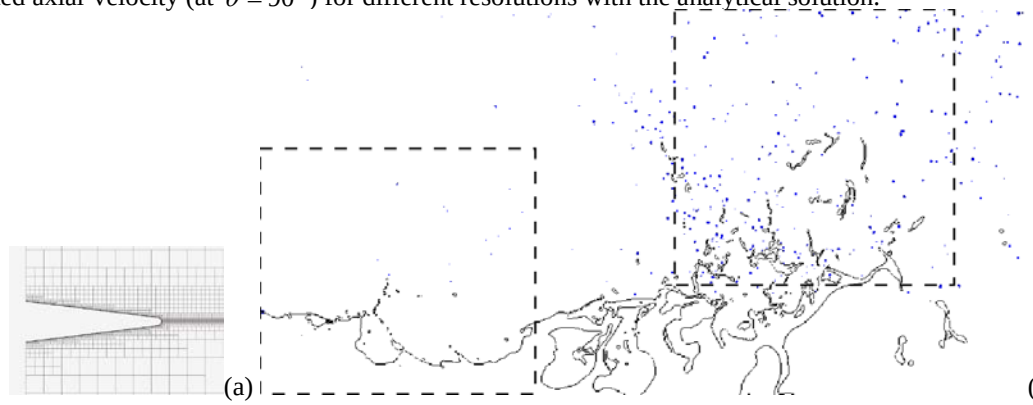

(a) (b)

Figure 3. (a) Shape of the nozzle separating the gas and liquid jets near the inlet. (b)Break up of a liquid jet by a high-speed coaxially flowing gas-jet. A cloud of small droplets, modeled as Lagrangian particles (shown in blue), formed during the atomization process are advected and spread by the high speed gas. The two dash boxes mark regions where we perform PDF of droplets.

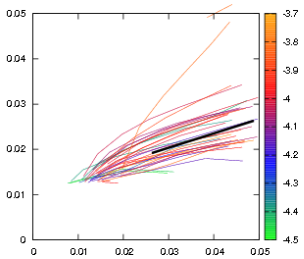

Figure 4. Trajectories of the particles formed near the nozzle-inlet (units in meters). The color of the trajectories correspond to logarithm of the particle diameter with the adjoining color-index. The dark line shows the mean-trajectory (~18^0).

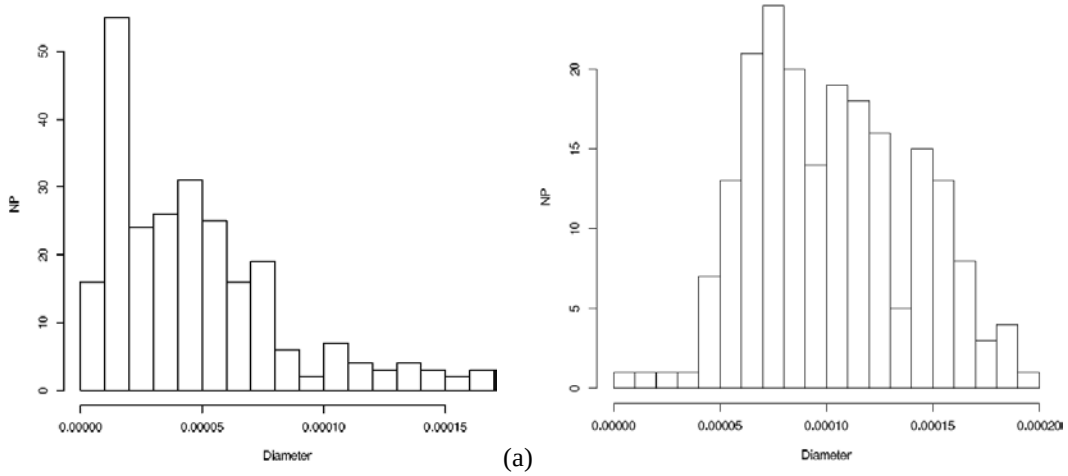

Figure 5. PDF of the diameter of the droplets formed at a location (a) near the nozzle-inlet (b) further downstream as marked in the Figure 4. The abscissa of the plots is the diameter of the droplet in meters.